CrystEngComm

PAPER

View Article Online
View Journal

Cite this: DOI: 10.1039/d6ce00062b

Spin-crossover iron(II) complexes featuring boronic acid and boronic ester groups: synthesis and magnetic properties

Minghui Zhang, Frank W. Heinemann and Marat M. Khusniyarov *

Received 22nd January 2026,
Accepted 2nd March 2026

DOI: 10.1039/d6ce00062b

rsc.li/crystengcomm

A series of bis(pyrazol-1-yl)pyridine (BPP) iron(II) complexes bearing either boronic acid or boronic monoester groups, with the general formula $[Fe^{II}(BPP)_2](ClO_4)_2$, have been synthesized and characterized in the solid state. The boronic acid or boronic monoester substituents are introduced at the 4-position of the pyridine ring. Despite their close structural similarity, the complexes exhibit markedly different magnetic properties. Complex **1a**, which contains boronic acid groups, undergoes an incomplete, thermally induced spin-crossover in the solid state. Conversion of the boronic acid groups into monomethyl or monoethyl esters stabilizes the high-spin state in **1b** and **1c**, respectively. Further substitution with electron-donating *tert*-butyl groups in **2b** enforces a pure low-spin state.

Introduction

Spin-crossover (SCO) complexes are known to be reversibly switched between two spin states in response to external stimuli such as light, heat or chemical environments.[1–4] Owing to their switching ability, SCO complexes have triggered significant interest over the past decades to develop responsive sensors,[5] and functional parts for molecular spintronics,[6] molecular electronics,[7] and memory devices.[8] A common class of SCO complexes comprises bis(pyrazol-1-yl) pyridine (1-BPP) based iron(II) complexes, which were developed and extensively studied by M. Halcrow and M. Ruben.[9–13] These complexes not only show SCO behaviour near room temperature,[14] but also feature 1-BPP ligands that can be readily functionalized at pyridine or pyrazole moieties, thus enabling the fine-tuning of the magnetic properties of corresponding metal complexes.[13,15–17]

Various modifications of 1-BPP-based iron(II) complexes have been synthesized and characterized; however, complexes featuring boronic acid groups have not yet been reported. We are particularly interested in boronic acid substituents, because they have demonstrated their potential in sensing applications, stemming from the vacant p orbitals on the boron centre.[18–22] The low-lying empty p orbitals can accept electrons from nucleophiles, resulting in the electron density enrichment of the boron centre as well as the geometry transformation from a trigonal planar to a tetrahedral structure.[22] Besides the Lewis acid character, boronic acids can also interact with small anions through two hydroxyl groups in the manner of Brønsted acids.[23] Moreover, boronic acids exhibit high affinity to biological molecules such as saccharides and dopamine, even under physiological conditions.[21,24] Upon reaction with these analytes, boronic acid esters are formed, leading, for instance, to a detectable reduction of fluorescence emission compared with the original boronic acids.[25]

The aforementioned characteristics have promoted us to explore the possibility of integrating boronic acid moieties into 1-BPP-based iron(II) complexes and further adjust the SCO behaviour of such complexes. The boronic acid group has been chosen to be attached at the pyridine C4 position because of synthetic simplicity as well as the electron-withdrawing nature of boronic acid, which can potentially lead to a temperature-induced SCO.[26] In this study, we demonstrate synthetic routes to 1-BPP-based iron(II) complexes functionalized with boronic acid groups and boronic esters. The first series of such complexes have been synthesized and their magnetic properties have been investigated.

Experimental section

All starting materials and solvents were used without further purification unless mentioned. Pure anhydrous solvents were collected from a Glass Contour solid-state solvent purification system (Irvine, CA). 4-Amino-2,6-bis(pyrazol-1-yl) pyridine, 4-bromo-2,6-bis(pyrazol-1-yl)pyridine, and 4-*tert*-butylpyrazole were synthesized following the literature reported methods.[27–29]

Department of Chemistry and Pharmacy, Friedrich-Alexander University Erlangen-Nürnberg (FAU), Egerlandstraße 1, 91058, Germany.
E-mail: marat.khusniyarov@fau.de

Instrumentation

Magnetic susceptibility data on solid samples were collected with a Quantum Design MPMS 3 magnetometer. DC susceptibility data were collected in the temperature range of 2–350 K for powder samples restrained with a polycarbonate gel capsule in an applied magnetic field of 1 T at a heating/cooling rate of 2 K min^{-1} and at 5 K intervals.

The magnetic susceptibility data were corrected for diamagnetism using the estimation $\chi_{m,diamag} = 0.5M_w \times 10^{-6}$ cm^3 mol^{-1} where M_w is the molar mass of compound.[30]

^{57}Fe Mossbauer spectra were recorded on a WissEl Mossbauer spectrometer (MRG-500) in constant-acceleration mode. ^{57}Co/Rh was used as the radiation source. The temperature of the samples was controlled by an MBBC-HE0106 Mossbauer He/N_2 cryostat within an accuracy of ±0.3 K. Isomer shifts were determined relative to the α-iron at 298 K. The program MX4w was used for the quantitative analysis of spectra.[31]

The NMR spectra were recorded with a JEOL ECX400 in rotating 5 mm o.d. tubes and processed using Delta V4.0 software provided by JEOL Ltd.

Powder X-ray diffraction patterns were obtained using a Bruker D8 diffractometer with a Cu Kα radiation source and a LyneEye XE-T detector. The IR spectra were recorded on a Shimadzu IRAffinity-1 system.

Crystallography

A suitable single crystal was embedded in protective perfluoropolyalkyl ether oil on a microscope slide, and a single specimen was selected and subsequently transferred to the cold nitrogen gas stream of the diffractometer. Intensity data were collected using MoKα radiation (λ = 0.71073 Å) on a Bruker Kappa PHOTON II IμS Duo diffractometer equipped with QUAZAR focusing Montel optics at a temperature of 100 K. The data were corrected for Lorentz and polarization effects, and semi-empirical absorption corrections were performed on the basis of multiple scans using SADABS.[32] The structures were solved by direct methods (SHELX XT)[33] and refined by full-matrix least-squares procedures on F^2 using SHELXL 2019/3.[34] All non-hydrogen atoms were refined with anisotropic displacement parameters. The positions of the oxygen-bound hydrogen atoms were determined from a difference Fourier map and their positional parameters were either refined (for **1a**, **1b**, and **1c**) or allowed to ride on their oxygen carrier atom (**2b**). All other hydrogen atoms were placed in optimized positions. The isotropic displacement parameters of all H atoms were tied to those of the corresponding carrier atoms by a factor of either 1.2 or 1.5. Olex2 was used to prepare the material for publication.[35]

Synthesis

4-((2,6-Bispyrazol-1-yl)pyridin-4-yl)boronic acid (L1). In a vacuum-heated Schlenk flask 4-bromo-2,6-bis(pyrazol-1-yl) pyridine (0.6 g, 2.07 mmol) was dissolved in 50 mL water-free tetrahydrofuran. Degassed water-free tributylborate (0.86 mL, 3.09 mmol) was added to the mixture *via* a syringe. The reaction mixture was then cooled down to −100 °C before a solution of 1.6 M *n*-butyllithium (1.8 mL, 2.88 mmol) was slowly added to the mixture. After stirring overnight, the reaction was quenched with 1 M aqueous hydrochloric acid (20 mL). The resulting mixture was carefully evaporated until THF was removed, whereupon a white solid precipitated from the aqueous phase. After drying *in vacuo*, **L1** was afforded as a white powder. Yield: 0.38 g, 71.8%. Elemental analysis calcd. for $C_{11}H_{10}BN_5O_2 \cdot 0.05H_2O$: C 51.62, H 3.98, N 27.36; found: C 51.52, H 3.81, N 27.20. ^{1}H NMR (400 MHz, DMSO-d_6, RT) δ: 8.94 ppm (d, ^3J = 2.5 Hz, 2H, H2), 8.76 (s, 2H, H5), 8.19 (s, 2H, H1), 7.87 (d, ^3J = 1.6 Hz, 2H, H4), 6.63 (dd, 2H, ^3J = 2.5 Hz, ^4J = 1.5 Hz, H3). ^{13}C NMR (400 MHz, DMSO d_6, RT) δ: 149.09 (C2), 142.41 (C4), 128.02 (C5), 113.60 (C3), 108.35 (C6) ppm; a carbon attached to the boron atom was not observed due to quadrupole broadening.

4-Amino-2,6-bis(4-*tert*-butylpyrazol-1-yl)pyridine. A 250 mL Schlenk round-bottom flask with an inert atmosphere was charged with 4-*tert*-butylpyrazole (6.00 g, 4.83 mmol) and 150 mL water-free diglyme. Sodium hydride (2.04 g, 5.1 mmol) was added to the reaction mixture. After hydrogen evolution ceased, 4-amino-2,6-dichloropyridine (3.20 g, 19.8 mmol) was added to the reaction mixture at RT. Afterwards, the reaction was heated to 160 °C for 3 days. The reaction was quenched by the addition of distilled water (150 mL), and the resulting yellowish solid was collected by filtration *via* a glass frit (Por. 3) without further purification. Yield: 5.22 g, 77.9%.

Elemental analysis calcd. for $C_{19}H_{26}N_6 \cdot 0.3C_6H_{14}O_3$: C 65.97, H 8.04, N 21.19; found: C 66.19, H 8.01, N 22.06.^{1}H NMR (400 MHz, $CDCl_3$, RT) δ: 8.27 (s, 2H, H2), 7.61 (s, 2H, H1), 7.05 (s, 2H, H3), 4.45 (S, 2H, H5), 1.30 (s, 18H, H-7).^{13}C NMR (400 MHz, $CDCl_3$, RT) δ: 156.84 (C1), 151.59 (C3), 140.02 (C6), 135.01 (C4), 123.06 (C5), 94.60 (C6), 31.72 (C7), 29.70 (C8) ppm.

4-Bromo-2,6-bis(4-*tert*butylpyrazol-1-yl)pyridine. In a 250 mL round-bottom flask 4-amino-2,6-bis(4-*tert*-butylpyrazol-1-yl) pyridine (3.00 g, 8.86 mmol), $NaNO_2$ (1.28 g, 18.6 mmol) and KBr (2.53 g, 21.3 mmol) were dispersed in 100 mL MeCN. Afterwards, 48% aqueous HBr (50 mL) was added dropwise into the mixture. After stirring for 3 h, the mixture was poured into a saturated Na_2CO_3 solution (200 mL). An orange solid precipitated from the mixture, which was collected by filtration *via* a glass frit (Por. 3) and washed with distilled water (50 mL) twice. The collected solid was air-dried overnight and purified *via* SiO_2 column chromatography using CH_2Cl_2/hexane (10 : 3) as the eluent (R_f = 0.3), yielding a white solid after solvent removal and dried *in vacuo.* Yield: 2.14 g, 60.2%.

Elemental analysis: calcd. for $C_{19}H_{24}N_6Br$: C 56.72, H: 6.01, N 17.41; found: C: 56.65, H: 6.10, N: 16.94.^{1}H NMR (400 MHz, $CDCl_3$, RT) δ: 8.24 (s, 2H, H2), 7.96 (s, 2H, H1), 7.66 (s, 2H, H3), 1.35 (s, 18H, H4).^{13}C NMR (400 MHz, $CDCl_3$, RT) δ: 150.77, 141.18, 136.45, 135.96, 122.96, 112.06, 31.62, 29.76 ppm.

((2,6-Bis(4-*tert*-butylpyrazol-1-yl))pyridin-4-yl)boronic acid (L4). A 100 mL Schlenk round-bottom flask with an inert atmosphere was charged with 4-bromo-2,6-bis(4-*tert*-

butylpyrazol-1-yl)pyridine (1.0 g, 2.5 mmol) and degassed THF (40 mL). Degassed tributylborate (1.04 mL, 3.75 mmol) was added. The mixture was cooled down to −100 °C before a solution of 1.6 M *n*-butyllithium (2.18 mL, 3.5 mmol) was slowly added *via* a syringe. After the reaction was stirred overnight, it was quenched by the addition of 1 M aqueous hydrochloride acid (20 mL). The resulting mixture was carefully evaporated until THF was removed, whereupon a white solid precipitated from the aqueous phase. The solid was collected by filtration *via* a glass frit (Por. 4) and washed with distilled water (10 mL) twice. The pure product was obtained after recrystallization from boiling toluene (300 mL) and drying *in vacuo* overnight at 65 °C. Yield: 0.83 g, 90.4%.

Elemental analysis: calcd. for $C_{19}H_{26}BN_5O_2$: C 62.14, H 7.14, N 19.07; found: C: 62.66, H: 7.14, N: 18.87.1H NMR (400 MHz, DMSO-d_6, RT) δ: 8.73 (s, 2H, H2), 8.60 (s, 2H, H4), 8.12 (s, 2H. H1), 7.81 (s, 2H, H3) ppm, 1.33 (s, 18H, H5). ^{13}C NMR (400 MHz, DMSO-d_6, RT) δ: 149.33, 140.38, 134.98, 123.30, 113.11, 112.17, 31.42, 29.35 ppm.

$[Fe^{II}(L1)_2](ClO_4)_2$ (1a). A solution of $Fe(ClO_4)_2{\cdot}6H_2O$ (50.5 mg, 0.14 mmol) in THF (5 mL) was added to a solution of L1 (100 mg, 0.39 mmol) in THF (5 mL) *via* a cannula under an inert atmosphere, whereupon an orange powder precipitated immediately. After the reaction was stirred for 3 hours at RT, the solvent was filtered. The residual solid was then washed with THF (2 mL × 2) and dried *in vacuo* overnight at 65 °C, affording 130 mg of powder (yield 87%). Crystals suitable for XRD were obtained from an acetone solution stored at room temperature for 7 days.

Elemental analysis calcd. for $C_{22}H_{20}N_{10}O_{12}B_2Cl_2Fe{\cdot}0.1C_4H_8O$: C: 34.84, H: 2.72, N: 18.14; found: C: 34.78, H: 2.92, N: 17.96.

$[Fe^{II}(L2)_2](ClO_4)_2$ (1b). The synthesis of **1b** was carried out using the same procedure as for **1a** but in methanol. The color of the reaction mixture changed to yellow, and a yellowish solid precipitated upon mixing. After stirring for 3 hours at RT, the solution was removed *via* a cannula filter. The residual solid was washed with methanol (2 mL × 2) and dried *in vacuo*, affording190 mg of a yellowish solid powder (yield: 63%). Crystals suitable for XRD were obtained by the slow diffusion of diethyl ether into a solution of **1b** in methanol over a period of 3 days. Elemental analysis calcd. for $C_{24}H_{24}O_{12}N_{10}B_2Cl_2Fe$: C: 36.35, H: 3.05, N: 17.66; found: C: 35.94, H: 3.24, N: 17.27.

$[Fe^{II}(L3)_2](ClO_4)_2$ (1c). The same reaction conditions as described for **1a** were employed but using ethanol as the solvent. 80 mg of a red solid was obtained by the slow diffusion of diethyl ether into ethanol solution (yield: 27%).

Elemental analysis calcd. for $C_{26}H_{28}O_{12}N_{10}B_2Cl_2Fe$: C: 38.04; H: 3.44; N: 17.06; found C: 38.18; H: 3.51; N: 16.92.

$[Fe^{II}(L4)_2](ClO_4)_2$ (2b). $Fe(ClO_4)_2{\cdot}6H_2O$ (48 mg, 0.136 mmol) was dissolved in 2 mL methanol. This solution was slowly added to a solution of **L4** (15 mL) in methanol *via* a cannula. The solution changed to a dark red colour immediately and no precipitate was observed. The reaction mixture was stirred for 3 h at room temperature. Afterwards, the volume of the reaction mixture was condensed to *ca.* 1/2. Crystals were obtained *via* the slow diffusion of diethyl ether into the mother liquor over a period of 3 days (yield 35%). Elemental analysis calcd. for $C_{40}H_{56}O_{12}N_{10}B_2Cl_2Fe{\cdot}0.6H_2O$: C: 46.73; H: 5.61; N: 13.62; found C: 46.38; H: 5.35; N: 13.98.

Results and discussion

Synthesis

The novel boronic acid-featured BPP ligands were prepared following a multistep synthesis (Scheme 1). First, deprotonation of pyrazole with sodium hydride afforded the corresponding pyrazolate salt **B**, which was subsequently used to substitute chlorides on compound **A**, giving the chelating aniline **C** (yield 90%). A copper-free Sandmeyer reactions with **C** yielded a bromo-derivative **D** (yield 61%).[28] Finally, the treatment of **D** with *n*-BuLi, the subsequent reaction with borate at low temperature, followed by acid-catalyzed hydrolysis produced the target tridentate ligand **L1** as a white powder with a 72% yield. Ligand **L4** was synthesized in a similar manner but starting with 4-*tert*-butylpyrazole, which was obtained by reacting *tert*-butylchloride and pyrazole in an autoclave at high pressure and high temperature for 2 days.[29]

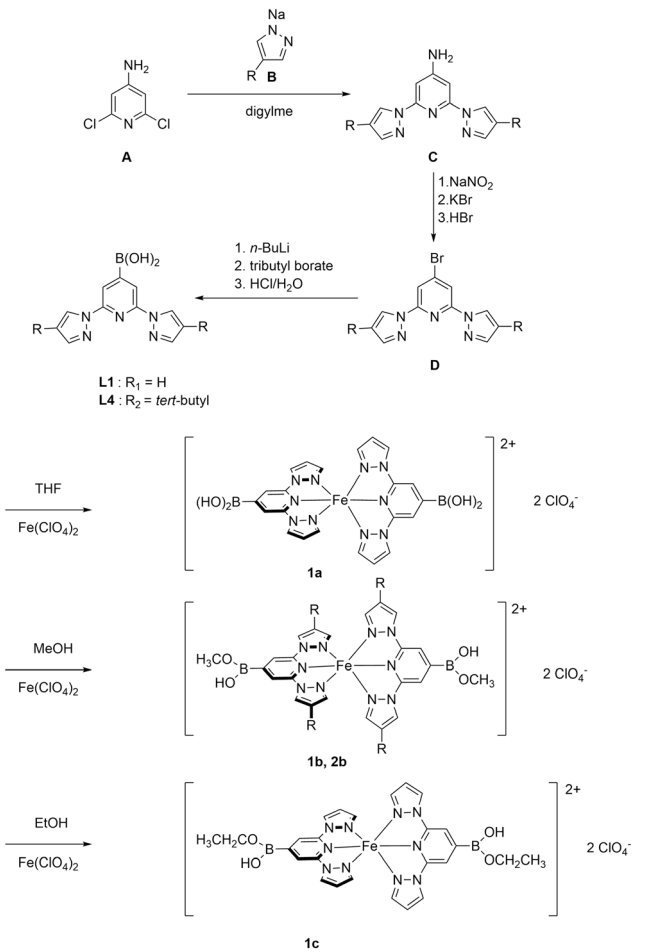

Scheme 1 Synthetic route for novel boronic acid-based BPP ligands and their iron(II) complexes.

Complex **1a** was prepared adopting literature-known methods.[36] Solutions of **L1** in THF and $Fe(ClO_4)_2{\cdot}6H_2O$ were mixed and stirred at room temperature for 3 h. An orange solid was precipitated from the solution and was collected by filtration. Due to the poor solubility of **1a** in common non-alcoholic solvents (note that **1a** decomposes in DMSO or DMF), we have attempted to crystalize **1a** in methanol and ethanol. Surprisingly, the obtained crystals **1b** and **1c** are modified complexes, where an esterification reaction took place giving methoxy and ethoxy monoesters, respectively (Scheme 2). The esterification of a single hydroxyl group of organic boronic acids in methanol is not uncommon.[37–40] If one of the hydroxyl group binds with nearby atoms through hydrogen bonds, the remaining hydroxyl group can undergo methylation in methanol. In our case, one of the hydroxyl group binds with perchlorate (*vide infra*), facilitating the esterification of the other. However, esterification in ethanol was first observed to the best of our knowledge. Subsequently, we have explored the possibility of direct synthesis of **1b** and **1c** in methanol and ethanol, respectively (Scheme 1). Similar synthetic procedures to those used for **1a** were performed, but in methanol and ethanol; **1b** precipitated as a bright yellow powder from the reaction, whereas red crystalline materials of **1c** were obtained *via* the slow diffusion of diethyl ether into the mother liquor.

In order to enhance the solubility of iron(II) complex **1a**, a *tert*-butyl moiety was introduced at the 3-position of pyrazole, as in ligand **L4** (Scheme 1). However, the solubility of the *tert*-butyl modified complex did not increase significantly, and we had to use alcoholic solutions here as well. The treatment of **L4** with $Fe(ClO_4)_2{\cdot}6H_2O$ in methanol leads to a red powder, which is proven to be **2b**-a complex featuring monoesters at both ligands. Additionally, we have sought to react **L1** with another commonly used iron precursor $Fe(BF_4)_2$. However, we are not able to purify this complex.

Crystal structures

Complex **1a** crystallizes in the monoclinic *C*2/*c* space group with 4 molecules and 1 water molecule per unit cell (Fig. 1). At 100 K, complex **1a** exhibits a distorted octahedral geometry, typically observed for this type of HS Fe(II) complex due to the Jahn–Teller effect.[41] The dihedral angel (θ) between the two ligand planes is significantly distorted from the ideal 90° to 77.8°, and the N(pyridyl)–Fe–N(pyridyl) angle (ϕ) reaches 155.8. The Fe–N bond lengths are in the range 2.1370(11)–2.1716(11) Å, further denoting a HS Fe(II) centre.[36] In the crystal structure, O–H···O hydrogen bonds are formed between boronic acid groups and nearby perchlorate anions. Each perchlorate anion bridges two boronic acid groups of neighbouring complex molecules within the lattice, thus leading to a polymeric chain structure along the crystallographic *b* axis. The introduction of an electron-withdrawing group at the pyridine C4 position is expected to favour the LS state according to Halcrow's work.[26] Analogue complexes with electron-withdrawing substituents such as cyanide, carboxylic acid and aldehyde groups at this position stabilize LS Fe(II) state.[12,42,43] However, our complex is a HS species. This discrepancy can be explained by the fact that the boronic acid group is less electron-withdrawing compared to the abovementioned substituents. Moreover, we assume that the highly distorted molecular structure of **1a** is the result of strong intermolecular interactions in the cell, which ultimately leads to the stabilization of the HS state.

Both mono-ester derivatives **1b** and **1c** crystallize in the *C*2/*c* space group with no solvent molecules in the unit cell (Fig. 2). The Fe(II) centres adopt HS configurations with typical long Fe–N bond lengths of 2.1269(16)–2.1873(18) Å and 2.1274(10)–2.1844(11) Å at 100 K, in **1b** and **1c**, respectively. Compared to the severely twisted molecular structure in **1a**, the distortions in **1b** and **1c** are moderate, supported by the observed N(pyridyl)–Fe–N(pyridyl) angles (ϕ) of 162.9° and 174.7° approaching the undistorted 180° as

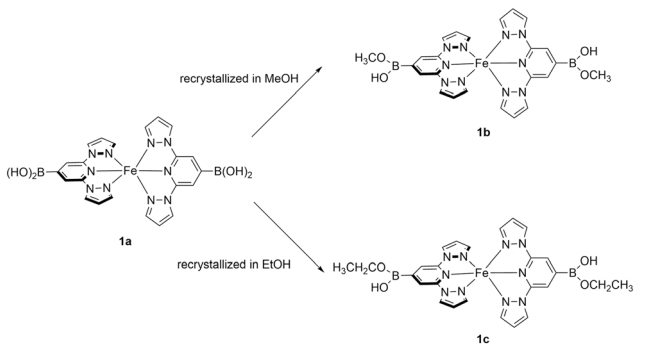

Scheme 2 Post-synthetic modification of **1a** giving monoester-derivatives **1b** and **1c**.

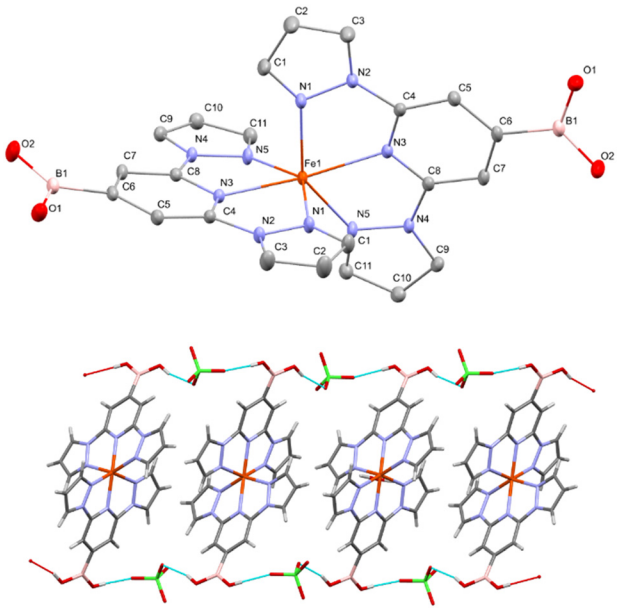

Fig. 1 Top: Molecular structure of **1a** at 100 K; the H atoms are omitted for clarity. Bottom: Crystal packing of **1a** showing a chain structure.

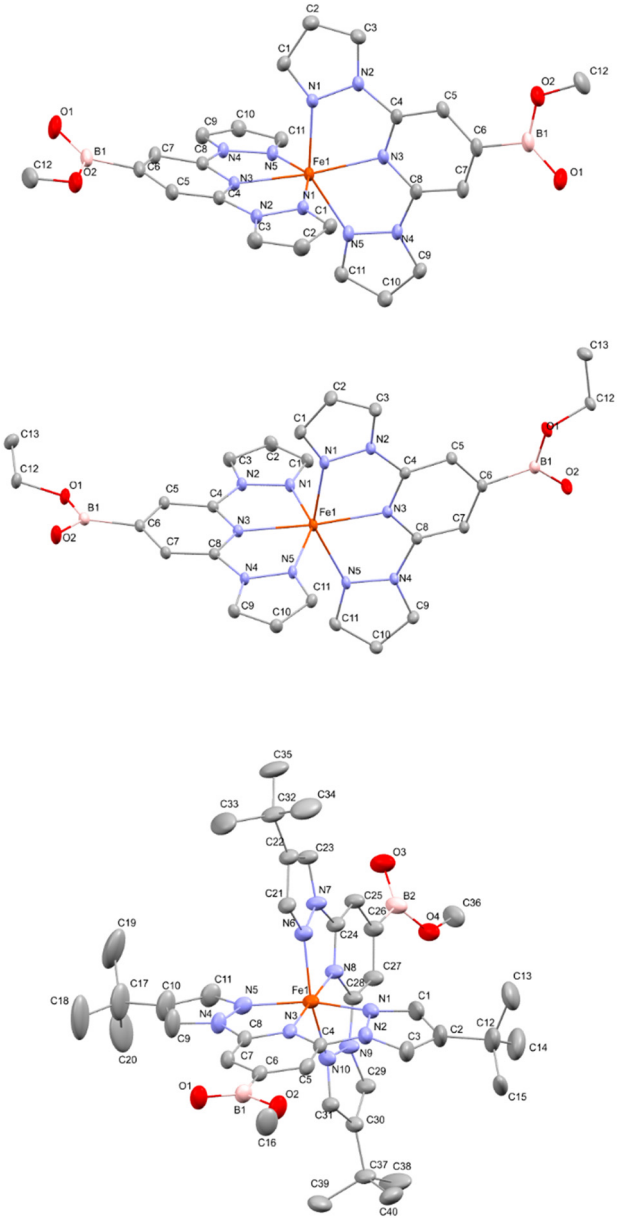

Fig. 2 Molecular structures of **1b** (top), **1c** (middle) and **2b** (bottom). The H atoms are omitted for clarity.

well as dihedral angles (θ) of 86.4° and 87.9° approaching the ideal 90° in **1b** and **1c**, respectively. The reduced distortion is likely due to the substitution of one of the hydroxyl groups with a methoxyl or ethoxyl group, respectively, and the concomitant reduction of intermolecular interactions. Indeed, only one hydrogen bond is formed per perchlorate cation and the polymeric structures disappear in **1b** and **1c**.

Two polymorphs of **2b** were observed from crystallization—red and yellow crystals, which is commonly observed for this class of compounds.[44–48] Despite numerous attempts, the crystal structures of the yellow crystals could not be determined due to very poor diffraction of the crystallized samples. The red polymorph crystalized in the monoclinic $P2_1/n$ space group and consists of two diethyl ether molecules per unit cell. Since the crystals degraded rapidly at room temperature due to solvent loss, we were able to determine the crystal structure only at low temperature. At 100 K, the Fe(II) centre reveals a low-spin (LS) Fe(II) state, as indicated by the shortened Fe–N bond lengths in the range of 1.899(21)–1.996(22) Å. The LS Fe(II) centre might be attributed to the electron-donating *tert*-butyl substituents at the pyridine 4-position strengthening the ligand field.[26] Selected bond distances and angular parameters for the crystal structures of this work are summarized in Table 1. A detailed summary of the crystallographic data is listed in the SI.

Magnetic properties

The magnetic properties, and consequently the spin states of the complexes, were investigated by SQUID magnetometry supported by ^{57}Fe Mössbauer spectroscopy. Complex **1a** undergoes partial, thermally induced SCO without hysteresis (Fig. 3). At room temperature (RT), **1a** reveals a χT product of 1.70 cm^3 mol^{-1} K (χ is the molar magnetic susceptibility), which is much lower than analogous pure HS Fe(II) complexes (3.3–3.8 cm^3 mol^{-1} K).[49] Upon heating to 350 K, χT increases to 2.35 cm^3 mol^{-1} K, corresponding to a thermally driven conversion of LS Fe(II) to HS Fe(II). Upon cooling to low temperature, χT gradually decreases to 0.96 cm^3 mol^{-1} K at around 100 K, reflecting a SCO from the HS to LS. A plateau at low temperature (30–100 K) suggests the presence of a residual HS fraction (around 25%). At 2 K, the χT product drops to 0.46 cm^3 mol^{-1} K, which is ascribed to the zero-field splitting of the remaining HS fraction. When slowly heated to RT, the SCO behaviour of **1a** follows the same behaviour as observed in the cooling mode, confirming reversible SCO without detectable hysteresis (SI).

Note that the spin state of **1a** determined from magnetic measurements (around 25% of the HS fraction at 100 K) is not in agreement with the crystallographic data, which indicates a pure HS state at 100 K. This is very likely due to the fact that magnetic measurements were performed on a powder sample, since we were not able to obtain enough crystalline materials for the magnetic measurements. So, the crystals and powder sample should represent two different phases. This has indeed been confirmed by measuring the powder XRD pattern of the powder sample, and comparing it with a simulated XRD pattern (see the SI).

Variable-temperature magnetic susceptibility measurements on complex **1b**, **1c** and **2b** were performed from 300 to 2 K. The measurement reveals that **1b** remains in the HS Fe(II) state at all temperatures, consistent with crystallographic data. At RT, the χT product of 3.78 cm^3 mol^{-1} K is higher than the spin-only value expected for an HS Fe(II) centre (3.0 cm^3 mol^{-1} K), but still coincides with values reported for similar HS Fe(II) complexes. Below 15 K, the χT product drops rapidly to 1.65 cm^3 mol^{-1} K because of the zero-field splitting at the $S = 2$ state for the HS Fe(II) ion. The variable temperature data χT was fitted with the PHI program,[50] which yields the g-value 2.24 and an axial zero-field splitting parameter D = 9.1 cm^{-1}.

Table 1 Selected bond distances (Å) and angular parameters (°) for the crystal structures measured at 100 K in this work

	1a	1b	1c	2b
Fe–N1	2.1716(11)–2.1716(12)	2.1873(18)–2.1873(18)	2.1844(11)–2.1844(11)	1.981(21)–1.986(21)
Fe–N3	2.1370(11)–2.1716(11)	2.1269(16)–2.1873(18)	2.1274(10)–2.1844(11)	1.899(21)–1.996(21)
Fe–N5	2.1635(11)–2.1636(11)	2.1685(18)–2.1685(18)	2.1943(11)–2.1943(11)	1.976(22)–1.996(22)
ϕ	155.8	162.9	174.7	177.7
θ	77.8	86.4	87.9	83.2

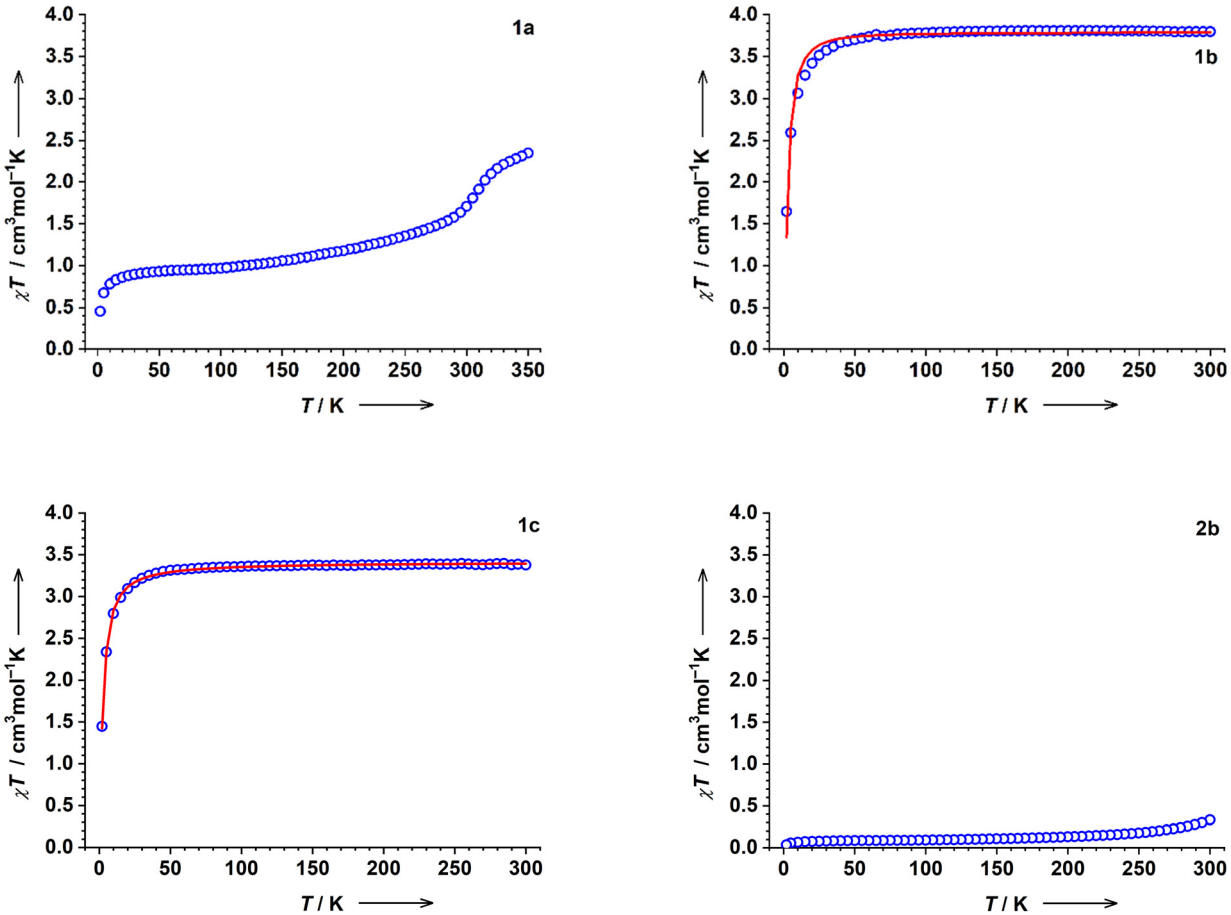

Fig. 3 Variable-temperature χT products of **1a** (top left), **1b** (top right), **1c** (bottom left) and **2b** (bottom right) at an external magnetic field of 1 T.

Likewise, complex **1c** reveals a pure HS Fe(II) state at all temperatures. At 300 K, the χT product of **1c** is 3.38 $cm^3\ mol^{-1}$ K, lower than **1b** and remains constant until 60 K. Upon further cooling, the χT product decreases sharply to 1.45 $cm^3\ mol^{-1}$ K at 2 K, again due to zero-field splitting. Fitting the variable temperature data yields g = 2.12 and a zero-field splitting parameter D = 7.0 cm^{-1}.

Magnetic measurements were also performed for **2b** over the 300–2 K range. Compound **2b** displays a χT product of 0.33 $cm^3\ mol^{-1}$ K at RT. The non-zero value is very likely due to minor paramagnetic impurities or a small fraction of the HS(II) species in the sample, which is very common for SCO Fe(II) species. Upon cooling, the χT product of **2b** gradually approaches 0.0 $cm^3\ mol^{-1}$ K at 4 K. The spin state of **2b** determined from magnetic measurements is in full agreement with the crystallographic data.

Our magnetic measurements have revealed that complex **1a** can potentially be used as a chemical sensor. At room temperature, **1a** reveals a mixed HS/LS state. When the boronic acid group is converted to a monomethyl ester, transforming the complex into **1b**, the material is switched to a pure HS state.

The boronic acid group can function as both a Lewis and a Brønsted acid, enabling interactions with small anions, diols, and various biological molecules.[23] Therefore SCO complexes featuring boronic acid groups are attractive candidates for sensing applications in solution. Upon analyte binding, magnetic properties might change, which can be

easily detected. In our case, complex **1a** shows very poor solubility and limited stability toward non-alcoholic solvents and water, and thus of little use for such applications. However, a series of complexes in this report clearly demonstrate that modifications at the boronic acid moiety can induce SCO, highlighting the potential of this class of complexes in designing magnetic molecular sensors.

Mössbauer spectroscopy

Zero-field ^{57}Fe Mössbauer spectroscopy was employed to confirm the oxidation and spin state of the iron centre in the complexes (Fig. 4). The Mössbauer spectrum of the SCO species **1a** reveals the coexistence of two distinct Fe(II) species at 77 K. A major quadrupole doublet (75%) exhibits an isomer shift (δ) 0.38 mm s^{-1} and a quadrupole splitting ($|\Delta E_Q|$) of 0.69 mm s^{-1}, in agreement with a LS Fe(II) state. A minor component (25%) exhibits an isomer shift of 1.18 mm s^{-1} and a quadrupole splitting of 3.03 mm s^{-1}, which is characteristic of a HS Fe(II) state. These Mössbauer measurements are in line with magnetic measurements.

Complex **1b** demonstrates (at 77 K) a single quadrupole doublet with an isomer shift of 1.14 mm s^{-1} and a quadrupole splitting of 2.82 mm s^{-1}, which is in agreement with a pure HS Fe(II) state. The Mössbauer measurement results are consistent with the magnetic measurements. Complex **1c** reveals one major HS Fe(II) component (90%) with an isomer shift of 1.12 mm s^{-1} and a quadrupole splitting of 3.42 mm s^{-1}, along with a minor impurity (10%) with an isomer shift of 0.36 mm s^{-1} and a quadrupole splitting of 0.78 mm s^{-1}. This impurity is identified as LS Fe(II) species, and despite many attempts to purify **1c**, we were not able to remove it completely. A plausible reason might be that a monoethyl ester is less stable than a monomethyl ester, and it slowly decomposes to a boronic acid. Thus, we concluded that the impurity here might be **1a**. The observed LS impurity can also explain the slightly lower χT product of **1c** at RT compared with **1b**.

The Mössbauer spectrum of **2b** measured at 77 K reveals a single quadrupole doublet with an isomer shift of 0.37 mm s^{-1} and a quadrupole splitting of 0.72 mm s^{-1}, identified as a LS

Table 2 Summary of Mössbauer parameters obtained at 77 K

	1a(LS)	**1a**(HS)	**1b**	**1c**	**2b**
δ, mm s^{-1}	0.38	1.18	1.14	1.12	0.37
$\|\Delta E_Q\|$, mm s^{-1}	0.69	3.03	2.82	3.42	0.72

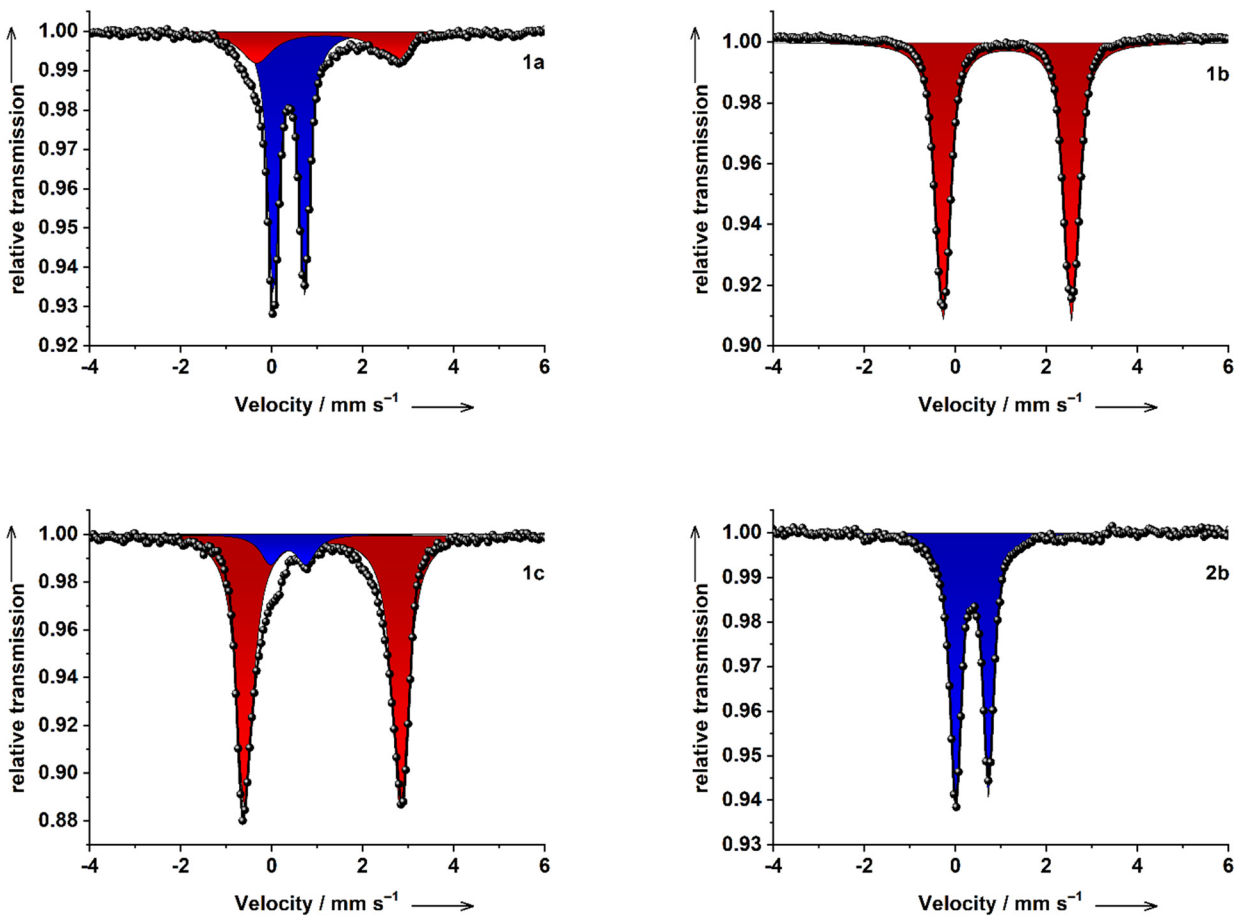

Fig. 4 Zero-field ^{57}Fe Mössbauer spectra measured on **1a** (top left), **1b** (top right), **1c** (bottom left) and **2b** (bottom right) at 77 K.

Fe(II) species, which is in full agreement with the magnetic measurements. A summary of the parameters from Mössbauer measurements are listed in Table 2.

Conclusions

Four bis(pyrazol-1-yl)pyridine iron(II) complexes featuring boronic acid or boronic monoester groups have been synthesized and their magnetic properties have been investigated. Minor changes of the ligand substituents allowed us to control the magnetic properties by moving from a pure low-spin complex with *tert*-butyl substituents over spin-crossover species with boronic acid substituents to pure high-spin complexes featuring boronic monoester substituents. The change in magnetic properties induced by esterification of the boronic acid group highlights the potential of such complexes for chemosensing applications. The low solubility of the obtained complexes, however, prevents such studies. The work on more soluble analogues is currently in progress in our laboratory.

Conflicts of interest

There are no conflicts to declare.

Data availability

Supplementary information (SI) is available. See DOI: https://doi.org/10.1039/d6ce00062b.

CCDC 2494923–2494926 contain the supplementary crystallographic data for this paper.[51a–d]

Acknowledgements

Dr. Andreas Scheurer is acknowledged for assistance with NMR measurements. Susanne Hoffmann is acknowledged for measuring powder XRDs. M. Z. is grateful to the China Scholarship Council for a stipend. M. M. K. thanks FAU Erlangen-Nürnberg and Prof. Karsten Meyer for providing access to spectroscopy facilities and continuous support. Deutsche Forschungsgemeinschaft is acknowledged for financial support (DFG Research Grants KH 279/6-1 and 279/8-1). This work is dedicated to Prof. Jörg Sundermeyer (Philipps-Universität Marburg) on the occasion of his retirement.

Notes and references

1 O. Kahn and C. Martinez, *Science*, 1998, **279**, 44–48.
2 P. Gütlich and H. A. Goodwin, *Spin crossover in transition metal compounds I-III, Topics in Current Chemistry*, Springer-Verlag, Berlin Germany, 2004, vol. 233–235.
3 M. A. Halcrow, *Spin-crossover materials: properties and applications*, John Wiley & Sons, Ltd, 2013.
4 M. M. Khusniyarov, *Chem. – Eur. J.*, 2016, **22**, 15178–15191.
5 S. Venkataramani, U. Jana, M. Dommaschk, F. D. Sonnichsen, F. Tuczek and R. Herges, *Science*, 2011, **331**, 445–448.
6 K. S. Kumar and M. Ruben, *Angew. Chem., Int. Ed.*, 2021, **60**, 7502–7521.
7 R. Torres-Cavanillas, M. Morant-Giner, G. Escorcia-Ariza, J. Dugay, J. Canet-Ferrer, S. Tatay, S. Cardona-Serra, M. Giménez-Marqués, M. Galbiati, A. Forment-Aliaga and E. Coronado, *Nat. Chem.*, 2021, **13**, 1101–1109.
8 G. Molnár, S. Rat, L. Salmon, W. Nicolazzi and A. Bousseksou, *Adv. Mater.*, 2018, **30**, 1703862.
9 M. A. Halcrow, *Coord. Chem. Rev.*, 2009, **253**, 2493–2514.
10 M. A. Halcrow, *New J. Chem.*, 2014, **38**, 1868–1882.
11 I. Šalitroš, O. Fuhr, R. Kruk, J. Pavlik, L. Pogány, B. Schäfer, M. Tatarko, R. Boča, W. Linert and M. Ruben, *Eur. J. Inorg. Chem.*, 2013, 1049–1057.
12 S. K. Kuppusamy, N. Del Giudice, B. Heinrich, L. Douce and M. Ruben, *Dalton Trans.*, 2020, **49**, 14258–14267.
13 N. Suryadevara, A. Mizuno, L. Spieker, S. Salamon, S. Sleziona, A. Maas, E. Pollmann, B. Heinrich, M. Schleberger, H. Wende, S. K. Kuppusamy and M. Ruben, *Chem. – Eur. J.*, 2022, **28**, e202103853.
14 M. A. Halcrow, *Coord. Chem. Rev.*, 2005, **249**, 2880–2908.
15 L. J. K. Cook and M. A. Halcrow, *Magnetochemistry*, 2015, **1**, 3–16.
16 V. García-López, M. Palacios-Corella, V. Gironés-Pérez, C. Bartual-Murgui, J. A. Real, E. Pellegrin, J. Herrero-Martín, G. Aromí, M. Clemente-León and E. Coronado, *Inorg. Chem.*, 2019, **58**, 12199–12208.
17 I. Galadzhun, R. Kulmaczewski, O. Cespedes, M. Yamada, N. Yoshinori, T. Konno and M. A. Halcrow, *Inorg. Chem.*, 2018, **57**, 13761–13771.
18 S. D. Bull, M. G. Davidson, J. M. Van den Elsen, J. S. Fossey, A. T. A. Jenkins, Y.-B. Jiang, Y. Kubo, F. Marken, K. Sakurai and J. Zhao, *Acc. Chem. Res.*, 2013, **46**, 312–326.
19 S. M. Butler, D. M. Beagan, W. Lewis, N. K. Szymczak and K. A. Jolliffe, *Angew. Chem., Int. Ed.*, 2025, 64e202502582.
20 P. A. Gale, E. N. Howe and X. Wu, *Chem*, 2016, **1**, 351–422.
21 Z. Guo, I. Shin and J. Yoon, *Chem. Commun.*, 2012, **48**, 5956.
22 R. Nishiyabu, Y. Kubo, T. D. James and J. S. Fossey, *Chem. Commun.*, 2011, **47**, 1106.
23 M. A. Martínez-Aguirre and A. K. Yatsimirsky, *J. Org. Chem.*, 2015, **80**, 4985–4993.
24 G. F. Whyte, R. Vilar and R. Woscholski, *ChemBioChem*, 2013, **6**, 161–174.
25 L. R. Ortega-Valdovinos, J. Valdes-García, I. J. Bazany-Rodríguez, J. C. Lugo-González, A. Dorazco-González and A. K. Yatsimirsky, *New J. Chem.*, 2021, **45**, 15618–15628.
26 L. J. K. Cook, R. Kulmaczewski, R. Mohammed, S. Dudley, S. A. Barrett, M. A. Little, R. J. Deeth and M. A. Halcrow, *Angew. Chem., Int. Ed.*, 2016, **55**, 4327–4331.
27 E. Nuin, W. Bauer and A. Hirsch, *Eur. J. Org. Chem.*, 2017, 790–798.
28 L. J. Kershaw Cook, H. J. Shepherd, T. P. Comyn, C. Baldé, O. Cespedes, G. Chastanet and M. A. Halcrow, *Chem. – Eur. J.*, 2015, **21**, 4805–4816.
29 A. L. Rheingold, L. M. Liable-Sands, J. A. Golan and S. Trofimenko, *Eur. J. Inorg. Chem.*, 2003, 2767–2773.
30 O. Kahn, *Molecular magnetism*, VCH Publishers, Inc., USA, 1993.

31 E. Bill, *MFIT, version 2.0*, MPI for Chemical Energy Conversion, Mühlheim/Ruhr, Germany, 2011.
32 SADABS, *Bruker AXS area detector scaling and absorption correction*, Bruker AXS, Inc, Madison WI., USA, 2014.
33 G. M. Sheldrick, *Acta Crystallogr., Sect. A: Found. Adv.*, 2008, **64**, 112–122.
34 G. M. Sheldrick, *Acta Crystallogr., Sect. C: Struct. Chem.*, 2015, **71**, 3–8.
35 O. V. Dolomanov, L. J. Bourhis, R. J. Gildea, J. A. K. Howard and H. Puschmann, *J. Appl. Crystallogr.*, 2009, **42**, 339–341.
36 L. J. Cook, R. Kulmaczewski, O. Cespedes and M. A. Halcrow, *Chem. – Eur. J.*, 2016, **22**, 1789–1799.
37 C. J. Davis, P. T. Lewis, D. R. Billodeaux, F. R. Fronczek, J. O. Escobedo and R. M. Strongin, *Org. Lett.*, 2001, **3**, 2443–2445.
38 M. Schwalbe, P. Wrzolek, G. Lal and B. Braun, *Eur. J. Inorg. Chem.*, 2014, 4209–4217.
39 J. Axthelm, H. Görls, U. S. Schubert and A. Schiller, *J. Am. Chem. Soc.*, 2015, **137**, 15402–15405.
40 W. Zhai, B. M. Chapin, A. Yoshizawa, H.-C. Wang, S. A. Hodge, T. D. James, E. V. Anslyn and J. S. Fossey, *Org. Chem. Front.*, 2016, **3**, 918–928.
41 L. J. K. Cook, R. Mohammed, G. Sherborne, T. D. Roberts, S. Alvarez and M. A. Halcrow, *Coord. Chem. Rev.*, 2015, **289**, 2–12.
42 A. Abhervé, M. Clemente-León, E. Coronado, C. J. Gómez-García and M. López-Jordà, *Dalton Trans.*, 2014, **43**, 9406–9409.
43 Q. Yang, Y.-S. Meng, T. Liu and J. Tang, *Dalton Trans.*, 2022, **51**, 602–607.
44 I. Šalitroš, J. Pavlik, R. Boča, O. Fuhr, C. Rajadurai and M. Ruben, *CrystEngComm*, 2010, **12**, 2361.
45 I. Šalitroš, O. Fuhr, A. Eichhöfer, R. Kruk, J. Pavlik, L. Dlháň, R. Boča and M. Ruben, *Dalton Trans.*, 2012, **41**, 5163.
46 I. Šalitroš, L. Pogány, M. Ruben, R. Boča and W. Linert, *Dalton Trans.*, 2014, **43**, 16584–16587.
47 I. Šalitroš, O. Fuhr and M. Ruben, *Materials*, 2016, **9**, 585.
48 S. K. Kuppusamy, A. Mizuno, L. Kämmerer, S. Salamon, B. Heinrich, C. Bailly, I. Salitros, H. Wende and M. Ruben, *Dalton Trans.*, 2024, **53**, 10851–10865.
49 J. Elhaïk, D. J. Evans, C. A. Kilner and M. A. Halcrow, *Dalton Trans.*, 2005, 1693–1700.
50 N. F. Chilton, R. P. Anderson, L. D. Turner, A. Soncini and K. S. Murray, *J. Comput. Chem.*, 2013, **34**, 1164–1175.
51 (*a*) CCDC 2494923: Experimental Crystal Structure Determination, 2026, DOI: 10.5517/ccdc.csd.cc2pr5d1; (*b*) CCDC 2494924: Experimental Crystal Structure Determination, 2026, DOI: 10.5517/ccdc.csd.cc2pr5f2; (*c*) CCDC 2494925: Experimental Crystal Structure Determination, 2026, DOI: 10.5517/ccdc.csd.cc2pr5g3; (*d*) CCDC 2494926: Experimental Crystal Structure Determination, 2026, DOI: 10.5517/ccdc.csd.cc2pr5h4.